Journal of Computational and Applied Mechanics, Vol. 8., No. 1., (2007), pp. 57–70

A NUMERICAL STUDY ON THE FREE-SURFACE CHANNEL FLOW OVER A BOTTOM OBSTACLE

Csaba Hős, László Kullmann
Budapest University of Technology and Economics (BUTE),
Department of Hydrodynamic Systems
1111 Budapest, Műegyetem rkp. 3.
csaba.hos@hds.bme.hu

[Received: March 19, 2007]

Abstract. This paper presents the results of a numerical study on a two-dimensional free-surface channel flow over a bottom obstacle. Of main interest is the capability of commercial CFD codes to solve such problems. ANSYS CFX 10.0 was used with its built-in two-phase flow model. While keeping the upstream water level in the channel constant, the downstream water level is systematically decreased, which results in increasing flow rate, supercritical flow, transcritical flow and weak hydraulic jump. The surface shapes of the subcritical CFD computations are compared to the results of the classic 1D theory. In the supercritical case, the parameters – wave crest and toe heights – of undular hydraulic jumps obtained by CFD are compared to the classic theory and to experimental results.

Keywords: open channel flow, undular hydraulic jump

1. Introduction

Free-surface flows and hydraulic jumps are important for environmental engineering (river flows, sediment distribution), ship engineering, water turbine engineering, etc. The actual problem motivating this paper was the need for open-surface channel modelling for the steady-state calculation of an urban water supply network. The basic concept was to verify the results of the model based on the classic 1D theory by means of 2D Computational fluid dynamics (CFD) simulations. Furthermore, the classic theory gives only a limited description of the flow but cannot handle e.g. supercritical cases. Also, there are parameters (notably the friction coefficient), which are hard to estimate. Finally, two-dimensional (and three-dimensional) effects are interest as understanding these issues might help to improve the simple 1D models.

The classic models on free-surface flows are based on the shallow water equations (see [1] or [2]), neglecting the deviation from the hydrostatic pressure distribution (vertical accelerations). These simple models are suitable only for purely subsonic or supersonic flows and more sophisticated models are needed for transonic flows and hydraulic jumps. A hydraulic jump is a spectacular phenomenon, with a lot of

turbulence, waves, unsteadiness and air entrainment, hence seems to be an appropriate test case for advanced numerical techniques of fluid mechanics.

Hydraulic jumps (analogous to shock waves in gas dynamics) are easily formed in free-surface flows as the wave velocity ($\sqrt{gh}$ in rectangular channels, h being the fluid depth) is often in the same order of magnitude as the flow velocity scale. The transition from supercritical to subcritical flows occurs via hydraulic jumps, through which the well-known 1D models describing the surface shape are not valid. Hydraulic jumps are not only challenging from the theoretical viewpoint (e.g. lack of an inviscid solution, deviation from the hydrostatic pressure distribution [3], presence of multiple scales [10]) but also raise problems in numerical modelling due to the sharp local gradient in the surface shape near the jump. Advanced numerical techniques employed to solve such problems start from finite difference methods [11], include local time stepping techniques [13] and generalised Riemann solvers [12] and attain full growth in the 3D RANS models as e.g. in [6] or [5]. Systematic measurements were also performed, see e.g. [3], [4], [9] and [8]. Ohtsu in [8] and Chanson in [9] give flow conditions for undular jump formation in terms of the Froude number (the ratio of flow and wave velocity) and channel width, consider Reynolds number effects, describe the main flow patterns and classify hydraulic jumps. They also report on the velocity and pressure distribution under the wave crests and at the wave toes.

The aim of the present paper is to test the capabilities of a commercial CFD code (ANSYS CFX 10.0) in terms of free-surface flows on a test case with subcritical and weakly supercritical flows. The paper is organised as follows. First, the classic theory is briefly summarised. Then, the CFD set-up (grid, turbulence model, boundary conditions, etc.) is presented. The results are split into two groups; subcritical and supercritical cases. The results of subcritical cases are compared to the classic 1D theory. The numerical results of the supercritical cases are finally compared to measurements.

2. **Theory**

In this section we briefly summarise some classic theoretical results of the corresponding literature. Consider the free-surface flow of an incompressible fluid in a channel of uniform width. In the case of steady-state behaviour, the losses in the flow (friction head loss) are compensated by the bottom slope. The flow is governed by the Bernoulli (energy) equation

$$\frac{d}{dx}\left(y + z + \frac{v^2}{2g} + h'\right) = 0, \tag{2.1}$$

where y denotes the water height, z represents the bottom contour and h' is the head loss. The continuity equation can be written as

$$Q = Byv = \text{const.} \tag{2.2}$$

with channel width B and average flow velocity v. Note that (2.1) assumes uniform velocity distribution (straight streamlines) and hydrostatic pressure distribution along

the depth. For most open-channel flows, the friction factor is independent of the Reynolds number and is only a function of the wall roughness. Its actual value is usually calculated by means of the Chézy rule by virtue of

$$\frac{dh'}{dx} = \frac{v^2}{C^2\, R_h}, \text{ where } C = R_h^{1/6}/n. \tag{2.3}$$

Here R_h is the hydraulic radius ($R_h = A/P$, i.e. wetted area over wetted perimeter) and n is a roughness coefficient having different values for different types of channel wall roughness.

Our study neglects 3D effects, thus only a segment of the flow with width B is considered, without side walls. We assume that $B \gg y$. Thus, $A = By$, $P = B$, $R_h = y$ and $q = yv\,[m^2/s]$. Inserting (2.2) and (2.3) into (2.1) we arrive at the ordinary differential equation for the water surface $y(x)$

$$\left(1 - \frac{q^2}{g\, y^3}\right) \frac{dy}{dx} = i - q^2\, n^2\, y^{10/3}, \tag{2.4}$$

where the new notation $i = -dz/dx$ was introduced. Note that if the term on the right-hand side vanishes, the slope of the surface does not change. This flow rate is called the normal flow rate and is given by

$$q_n = \frac{i\, y^{10/3}}{n}. \tag{2.5}$$

On the other hand, if the term on the left-hand side vanishes, the slope of the surface becomes infinite. Let us rewrite this term as

$$1 - \frac{q^2}{g\, y^3} = 1 - \left(\frac{v}{\sqrt{gy}}\right)^2 = 1 - Fr^2. \tag{2.6}$$

The Froude number Fr is the ratio of the fluid and wave velocity and is analogous to the Mach number in gas dynamics. As $Fr \to 1$, $dy/dx \to \infty$, which is not possible. Indeed, with a strongly curved water surface, the assumptions of straight streamlines and hydrostatic pressure variations are no longer valid. If $Fr < 1$, the flow is called subcritical while if $Fr > 1$, the flow is called supercritical.

The transition from subcritical to supercritical flow (or vice versa) cannot be computed by means of (2.4). Instead, let us apply the frictionless momentum equation, i.e.

$$\frac{v_1^2}{g} y_1 + \frac{y_1^2}{2} = \frac{v_2^2}{g} y_2 + \frac{y_2^2}{2}. \tag{2.7}$$

By making use of the continuity equation, it is easy to show that

$$\frac{y_2}{y_1} = \frac{1}{2}\left(\sqrt{1 + 8\, Fr_1^2} - 1\right). \tag{2.8}$$

Equation (2.8) gives the connection between the upstream and downstream velocities and water heights across a hydraulic jump, where subscript '1' refers to the upstream side and subscript '2' to the downstream side of the jump.

3. **CFD setup**

The commercial computational fluid dynamics code ANSYS CFX 10.0 was used for 2D steady-state numerical simulation. The set of equations solved by CFX 10.0 are the unsteady Reynolds-averaged Navier-Stokes equations in their conservation form, see [7] for details. An additional general transport equation is solved for each component's volume fraction. The total length of the bottom obstacle was $L = 0.355m$ (see Figure 1) and the computational domain stretched $3L$ length before and $10L$ after the obstacle. The height of the domain was $0.5m$. A two-dimensional structured mesh was created, with a thickness of $0.01m$ in the span-wise direction. Mesh sensitivity tests were performed with three different mesh densities on the same blocking structure and the middle one containing approx. 25k of cells was found to be adequate. (These results are not reported here; the difference in mass flow rate was below 1% for the middle and the finest mesh. The computational effort on the finest mesh was almost unbearable; a typical computation needed approx. 6 days on our 2.4 GHz PC with 1GB RAM.) Due to visibility reasons, a blow-up of the *coarsest* mesh close to the obstacle is shown in Figure 2. The actual (middle) mesh used in the computations contained a four times denser mesh in the vertical direction and a twice denser one in the horizontal direction. The cell aspect ratio was between 0.025 and 0.9996, the skewness was between 0.646 and 1.000 and the maximal volume ratio was between 1.0004 and 4.9.

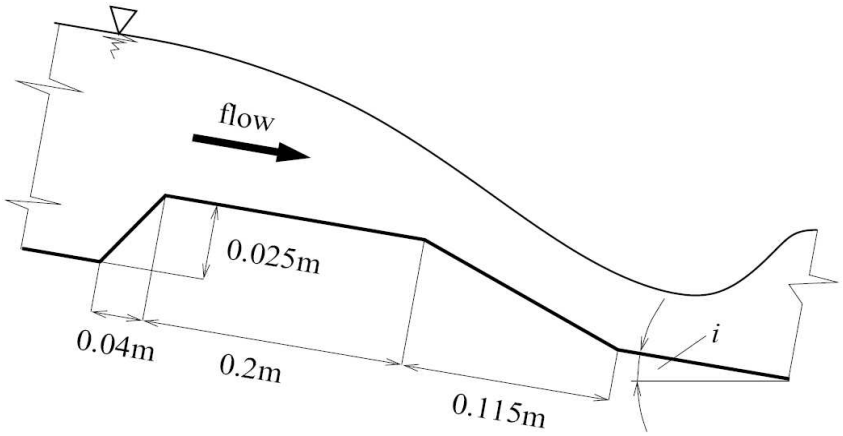

Figure 1. Geometry of the bottom obstacle

The inclination of the bottom was set to $i = 3 \times 10^{-4}$, which was taken into account by defining the appropriate components of the gravity force g_x and g_y. Water level boundary conditions were set on the upstream and downstream side prescribed through hydrostatic pressure profiles. A rough wall with $0.5\,mm$ wall roughness was set for the channel bottom and an opening boundary condition with a uniform static pressure of $1\,bar$ was set for the upper boundary. A high resolution spatial difference

scheme was applied and a relatively small, $0.01\,s$ physical time step was prescribed. Note that as the wave velocity was typically $1.32\,m/s$ ($y_u = 0.18\,m$) and the overall length of the computational domain was $4.97\,m$, the characteristic time was $3.73\,s$. Yet numerical experiments showed that a maximal time step of $0.01\,s$ was needed for stable simulation, which resulted in a large number of iterations, typically between 5000 and 10000. The convergence was judged by means of mass flow rate balance at the inlet and outlet because it was found that during the computations, the usual convergence criteria for the residuals (typically, 10^{-5}) do not guarantee a mass balance error smaller than 0.1%. A homogenous multiphase model was used, which handles the two phases as a single mixture with different volume fractions. The surface tension, interphase mass transport and interphase forces were neglected. A standard $k - \epsilon$ turbulence model was adopted.

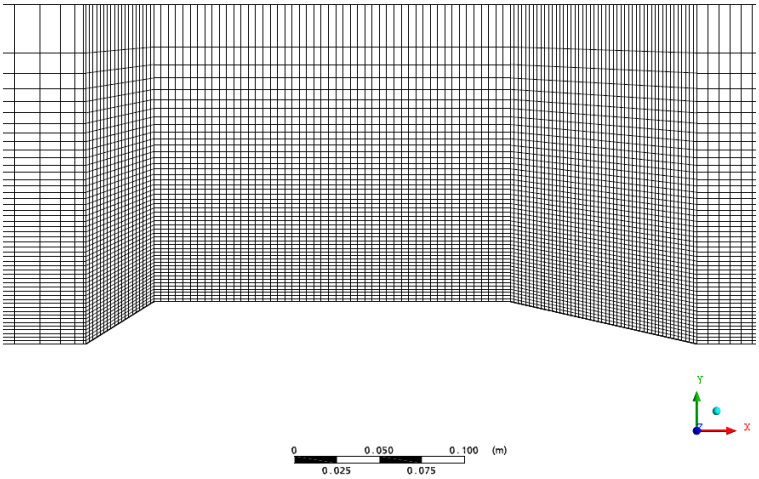

Figure 2. The coarsest computational mesh close to the obstacle, see text for details

4. **Overview of the results**

Table 1 gives a general overview of the simulations. The upstream water height was kept constant at $y_u = 0.18\,m$ while the downstream water height was decreased systematically, from $y_d = 0.18\,m$ to $y_d = 0.11\,m$. The water surface is defined as an isosurface with 50% volume fraction of water. The water surface shapes are depicted in Figure 3.

The very first simulation with the same upstream and downstream water level allows us to calculate the normal flow rate and thus to identify the wall roughness parameter n defined in (2.3), which was found to be $n = 0.0149$. Note that this value is consistent with the literature, e.g. for smooth metal flumes, cement mortar surfaces or unplaned plank flumes, [14, p. 435] gives $n = 0.011 \ldots 0.015$.

Table 1. Summary of the CFD runs. †: indicates that the undular jump stretched outside the computational domain. For all calculations $y_u = 0.18m$.

$y_d\,[m]$	$Q \times 10^3\,[m^3/s]$	$Fr_{max}\,[-]$	Comment
0.180	0.667	0.334	subcritical
0.175	1.104	0.630	subcritical
0.170	1.256	0.791	subcritical
0.160	≈1.410	≈0.958	unstable
0.155	1.402	1.076	undular jump
0.150	1.422	1.236	undular jump
0.145	1.429	1.415	undular jump
0.140	1.432	1.411	undular jump
0.130	1.463	1.402	undular jump †
0.120	1.487	1.395	undular jump †
0.110	1.529	1.349	undular jump †

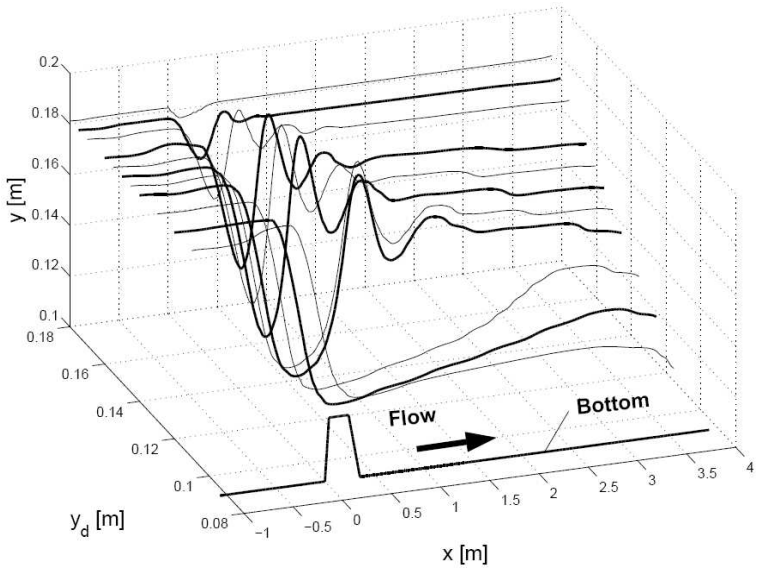

Figure 3. Fluid surface shapes for several downstream water heights (see Table 1 for the actual values). The different line widths are only for visibility reasons

As the downstream water level was decreased, the flow rate increased. Calculating the maximal Froude number along the channel shows that the subcritical/supercritical transition occurs at approx. $y_d = 0.16\,m$. Indeed, this calculation was unstable and only approximate values of flow rate and Froude number were obtained. (By 'unstable'

a periodic oscillation with an amplitude of about 10% of the flow rate is meant. During the oscillation, the RMS value of the residuals was continuously below 10^{-5}.)

By decreasing the downstream water height below $0.16\,m$, the flow became supercritical. As it is known from the literature (e.g. [3]), for small Froude numbers of $1 < Fr < 1.7$, undular jumps are formed. In the last three simulations, the Froude number was between 1.4 and 1.35 yet no undular jumps were observed, which is probably due to the insufficient length of the computational domain in the downstream direction. This issue needs further study and the analysis of these results is not addressed in this paper, however for the sake of completeness, the main parameters of these runs and the corresponding surface shapes are also given.

5. **Analysis of the subsonic results**

In the case of subcritical flow (the first three simulations in Table 1), the CFD results are compared to the surface predicted by the 1D model. The ordinary differential

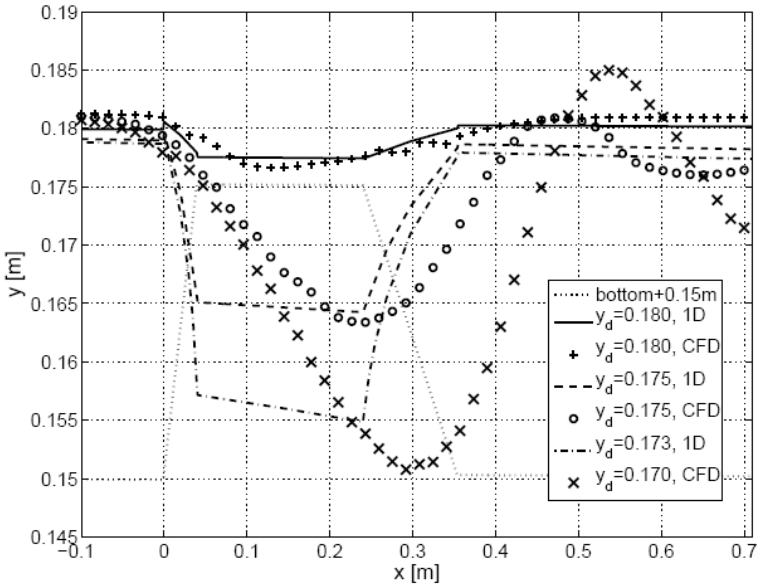

Figure 4. Subcritical computations, comparison of 1D model and CFD results. Note that for better visibility, the bottom obstacle was shifted by $0.15\,m$ in the y (vertical) direction

equation (2.4) together with the upstream and downstream water heights defines a boundary value problem with two boundary conditions and one free parameter, namely the flow rate. The problem was solved with Matlab's boundary value solver `bvp4c`. The roughness parameter n was kept constant (0.0149) during the calculations. The 1D model predicts the subcritical/supercritical transition to $y_d \approx 0.172\,m$, thus

the solution obtained with $y_d = 0.173\,m$ was plotted vs. the CFD result with $0.17\,m$. Note that the boundary value problem was solved on the same domain as the CFD calculations (total length of 14 times the obstacle length) but for better visibility, only the region close to the obstacle is presented in Figure 4.

As the flow rate increases (y_d decreases), an increasing difference between the 1D model and the CFD results is observed. The main reason for this increasing deviation is the increasing curvature of the streamlines and thus the loss of validity of the 1D assumptions (uniform flow profile, hydrostatic pressure distribution). It is also interesting that the 1D model predicts much sharper surfaces and the wavy contour after the obstacle is missed. This suggests that although (2.4) remains physically meaningful up to $Fr = 1$, it provides acceptable results only for a much narrower range of the Froude number, i.e. for flows with a slightly curved surface.

6. **Analysis of the supercritical results**

For slightly supercritical flows with $1 < Fr_1 < 1.7$ undular jumps are formed, see e.g. [9] for details. The situation is sketched in Figure 5: the supersonic ($Fr_1 > 1$) upstream flow slows down to subsonic flow via a hydraulic jump. As the energy is not dissipated by rollers or regions of high turbulence intensity, the energy losses are radiated forward in a train of stationary waves. The most important parameters are the Froude number and the water height at the toe of the jump and at the first wave crest. According to the classic 1D theory, these values are connected by (2.8).

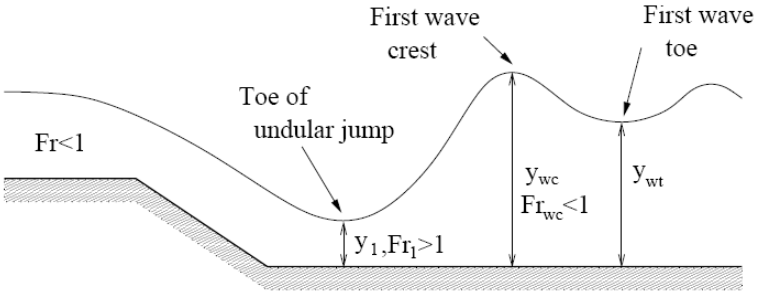

Figure 5. Parameters of the undular hydraulic jump

The experiments of Ohtsu et al. [8] are used as reference for validating the computations. Also, some preliminary measurements were performed on the recently built channel of the Department of Hydrodynamic Systems but as the experimental rig is not yet fully set up these results are only for rough checking. The authors in [8] give the following conditions for the classification of undular jumps (UJ): $1 \le Fr_1 \le Fr_{1limit}$ for breaking UJ and $Fr_{1limit} \le Fr_1 \le Fr_{1u}$ for nonbreaking UJ, where

$$Fr_{1limit} = 1.79 - 0.03\,(10 - B/y_1)^{1.35}\,, \tag{6.1}$$

$$Fr_{1u} = 2.10 - 0.03\,(12 - B/y_1)^{1.35}\,, \tag{6.2}$$

with $2 \leq B/y_1 \leq 10$ and $2 \leq B/y_1 \leq 12$ for (6.1) and (6.2), respectively. Here B is the channel width. As only 2D simulations were performed in this study, we use the largest value of the B/y_1 values, which gives $Fr_{1limit} = 1.78$ and $Fr_{1u} = 2.1$. Indeed, the largest Froude number (at the toe of the UJ) in the simulation was 1.457 and undular jumps were observed in the computations.

Let y_{wc} denote the height of the first wave crest and y_{wt} stand for the height of the first wave toe, see Figure 5. Then, according to [8], we have

$$\frac{y_{wc}}{y_1} = -0.76\,(Fr_1 - 1)^2 + 2.3\,(Fr_1 - 1) + 1, \tag{6.3}$$

$$\frac{y_{wt}}{y_1} = 0.90\,(Fr_1 - 1)^{2.5} + 0.2\,(Fr_1 - 1) + 1. \tag{6.4}$$

Table 2 presents the comparison between the CFD results, (2.8) (with $y_2 = y_{wc}$) and Ohtsu's formula (6.3) from [8]. The water heights at the first wave crest predicted by the classic theory and those of the CFD computations agree well. Note that as the energy dissipation in undular jumps is very low, the classic analytical formula (2.8) is well applicable. From the CFD point of view, as wild recirculation zones with high turbulence intensity and air entrainment (e.g. rollers) are not present, turbulence modelling is not a primary issue and also as the interface of the two phases remains well-defined (no air entrainment or bubble formation), there is no need for inhomogeneous multiphase models. Ohtsu's formula slightly overpredicts the height but it should be emphasised that this formula has been developed for a much wider Froude number range.

Table 2. Undular hydraulic jump: comparison of the classic theory, CFD results and Ohtsu's formula (6.3) in [8]

y_d [m]	y_1 [m]	Fr_1 [–]	Fr_{wc} [–]	y_{wc}/y_1, (2.8) [–]	y_{wc}/y_1, CFD [–]	y_{wc}/y_1, (6.3) [–]
0.155	0.1192	1.179	0.617	1.241	1.233	1.387
0.150	0.1091	1.310	0.631	1.419	1.412	1.640
0.145	0.1010	1.460	0.678	1.624	1.624	1.897
0.140	0.0970	1.457	0.684	1.620	1.690	1.892

Figures 6 and 7 provide a visual interpretation of Table 2. Starting with Figure 6, we conclude again that the CFD results show a satisfactory agreement with the classic theory (2.8) while (6.3) gives slightly larger values. It is not clear for the authors why (6.3) is inconsistent with (2.8): at least for the $Fr_1 \to \infty$ limit (6.3) should tend asymptotically to (2.8). Due to the uncertainties in water level measurement, the experimental results are hard to judge. The error in the height measurement is estimated to be 3 mm, the velocity measurement (performed with a metering orifice) is loaded with max. 1% error. This results in a relative error in Fr_1 between 2.7% and 5.7%, and 6.3 . . . 13.3% in y_{wc}/y_1 and y_{wt}/y_1.

The parameters of the first wave toe depicted in Figure 7 are again very hard to judge. On one hand, the measurements are close to Ohtsu's formula (6.4) apart from

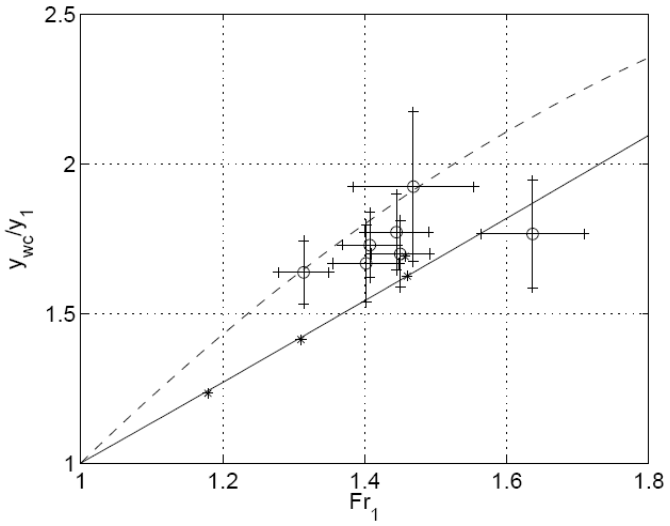

Figure 6. Dimensionless wave crest height vs. upstream Froude number. Circles denote measurement, the asterisk stands for CFD results, the continuous line is (2.8) and the dashed line is (6.3)

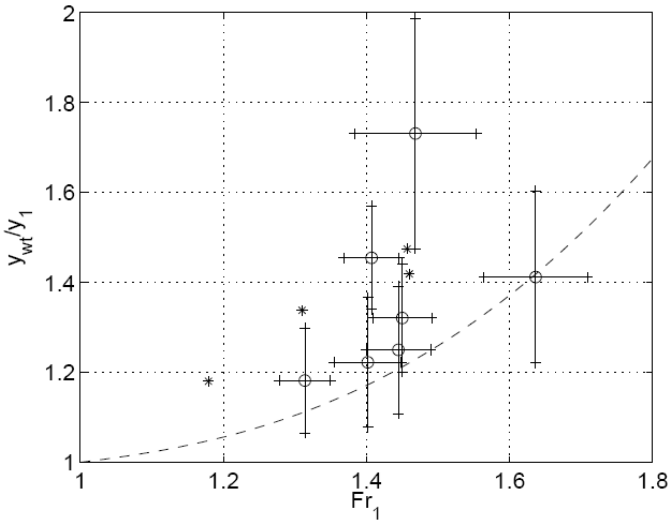

Figure 7. Dimensionless wave toe height vs. upstream Froude number. Circles denote measurement with error bars, the asterisk stands for CFD results and the dashed line is (6.4)

the two points of high w_{wt}/y_1. On the other hand, the measurements and Ohtsu's results do not coincide with the CFD results but it is not clear that if CFD predicts the first wave crest height properly, why should it miss the first wave toe. However, one should be aware that during the post-processing of the CFD results, another uncertainty is introduced: the extracted water heights depend on the volume fraction level through which the surface is defined (50% in this paper): by varying the volume fraction level (say, to 90%), the surface also changes. This issue needs further study and notably a systematic CFD study coupled with experiments.

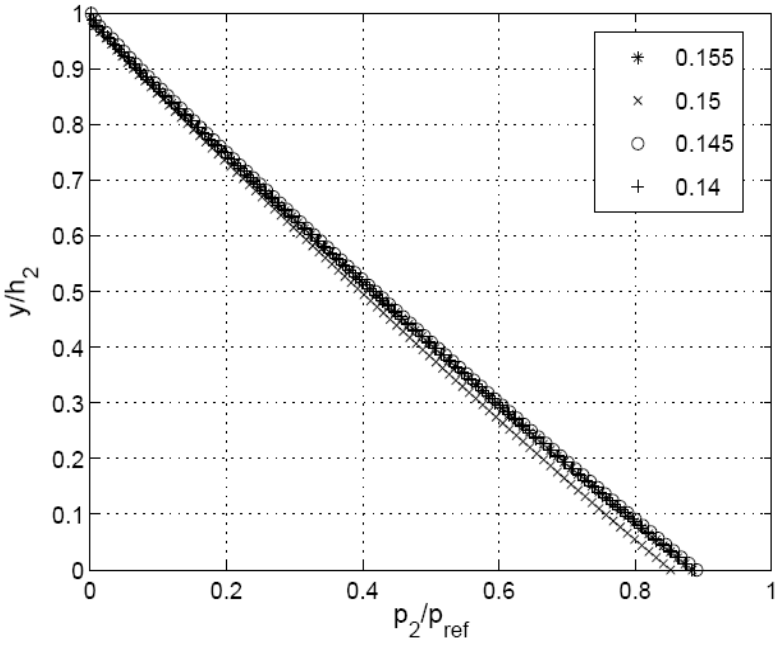

Figure 8. Dimensionless pressure distribution vs. dimensionless depth at the crest of the first wave. The parameters in the legend refer to y_d

Next, the pressure distributions are studied. Figures 8 and 9 depict the dimensionless pressure distributions across the depth at the toe of the jump and at the first wave crest. The reference pressure was set to $p_{ref} = \rho\, g\, y_{wc}$ and $p_{ref} = \rho\, g\, y_{wt}$ (respectively), i.e. the hydrostatic pressure according to the water height. The results are in good accordance with [4] and [15], especially the profiles beneath the first wave crest. Clearly, the pressure distribution is not hydrostatic beneath the undulations; the pressure gradients were larger when the free-surface was curved upwards (i.e. concave) and less than the hydrostatic gradient when the surface was convex. Note that no recirculation zones have been observed in these calculations. For the last two cases ($y_d = 0.145$ and $y_d = 0.14$) the hydrostatic pressure distribution was regained at the

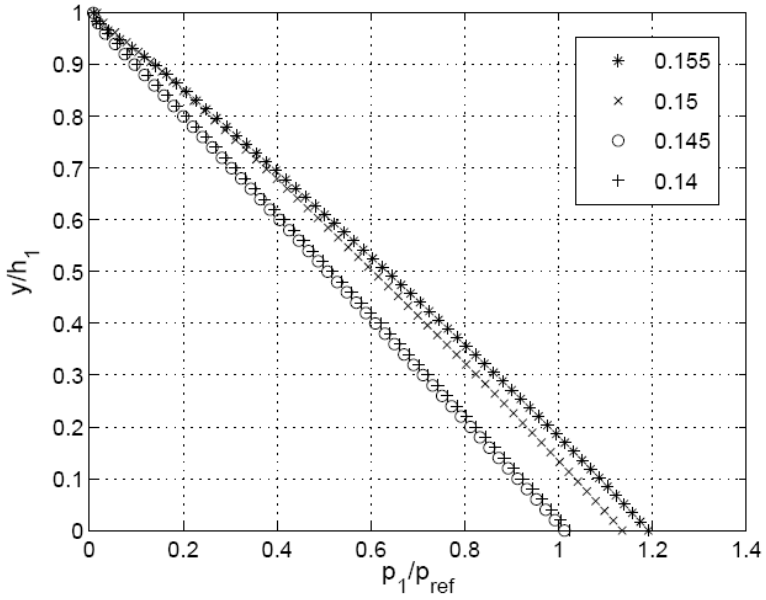

Figure 9. Dimensionless pressure distribution vs. dimensionless depth at the toe of the hydraulic jump. The parameters in the legend refer to y_d

toe of the jump, however, for $y_d = 0.155$ and $y_d = 0.15$ a higher pressure gradient has been observed. Figure 10 provides a visual interpretation of the highly curved streamlines in the undular hydraulic jump.

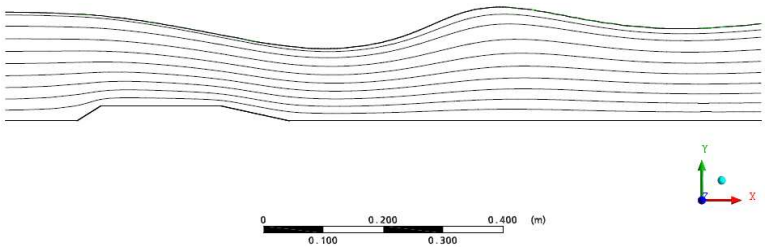

Figure 10. Streamlines beneath the undular jump, $y_d = 0.145m$

7. **Conclusions**

It was shown that commercial CFD codes offer the possibility of analysing free-surface flows without differentiating between or separately modelling subcritical, transcritical and supercritical cases. The price is the computational effort: one steady-state run

for the problem presented would require 10-15 hours of computation on a 2.4 GHz PC with 1GB RAM. Two-dimensional features of such flows were highlighted, notably non-hydrostatic pressure distribution. Weak hydraulic jumps (undular jumps) were studied; classic theory, recent experiment-based formulae, CFD results and experiments were compared. Although several questions have not yet been solved (e.g. why CFD and measurement do not coincide at the first wave toe), it is clear that commercial CFD codes – under careful supervision – are useful tools for analysing such problems. However, whether stronger jumps (larger Fr numbers) with wilder transition zones, air entrainment and unsteady phenomena can be analysed with such numerical techniques is an issue the authors wish to study in the future.

REFERENCES

1. Fox, R.W. and McDonald, A.T.: *Introduction to Fluid Mechanics*. John Wiley & Sons, (1995), ISBN: 0-471-59274-9.
2. Halász, G., Kristóf, G. and Kullmann, L.: Flow in Pipe Systems, Műegyetem Kiadó, (2002), ISBN: 963-420-708-1 (in Hungarian).
3. Svendsen, IB.A., Veeramony, J., Bakunin, J. and Kirby, J.T.: The flow in weak turbulent hydraulic jumps, *Journal of Fluid Mechanics*, **418**, (2000), 25-57.
4. Chanson, H.: Boundary shear stress measurements in undular flows: Application to standing wave bed forms. *Water Resources Research*, **36**(10), (2000), 3063-3076.
5. Metcalf, B., Longo, J., Ghosh, S. and Stern, F.: Unsteady free-surface wave-induced boundary-layer separation for surface-piercing NACA-0024 foil: Towing tank experiments. *Journal of Fluids and Structures*, **22**, (2006), 77-98.
6. Rhee, S.H., and Stern, F.: RANS model for spilling breaking waves. *Journal of Fluids Engineering*, **124**, (2002), 424-432.
7. Ansys Inc.: CFX 10 Users' Manual, (2006).
8. Ohtsu, I., Yasuda, Y. and Gotoh, H.: Flow conditions of undular hydraulic jumps in horizontal rectangular channels. *Journal of Hydraulic Engineering*, **129**, (2003), 948-955.
9. Chanson, H.: Characteristics of undular hydraulic jumps: experimental apparatus and flow patterns. *Journal of Hydraulic Engineering*, **121**(2), (1995), 129-144.
10. Steinruck, H., Schneider, W. and Grillhfer, W.: A multiple scale analysis of the undular hydraulic jump in turbulent open channel flow. *Fluid Dynamics Research*, **33**, (2003), 41-55.
11. Zeruhin, Y.T. and Fenton, J.D.: One-dimensional simulation model for steady transcritical free surface flows at short length transitions. *Advances in Water Resources*, **29**, (2006), 1598-1607.
12. Birman, A. and Falcvitz, J.: Application of the GRP scheme to open channel flows. *Journal of Computational Physics*, (2006), doi:10.1016/j.jcp.2006.07.008.
13. Crossley, A.J., Wright, N.G. and Whitlow, C.D.: Local time stepping for modelling open channel flows. *Journal of Hydraulic Engineering*, (2003), doi:10.1061/(ASCE)0733-9429 (2003)129:6(455).

14. Daugherty, R.L., Franzini, J.B. and Finnemore E.J.: *Fluid Mechanics with Engineering Applications*. McGraw-Hill Book Company, Singapore, (1989), ISBN:0-07-100405-X.

15. Chanson, H.: Physical modelling of the flow field in an undular tidal bore. *Journal of Hydraulic Research*, **43**(3), (2005), 234-244.